Science Advances
AAAS

advances.sciencemag.org/cgi/content/full/4/8/eaar3230/DC1

Supplementary Materials for

Multiplexed oscillations and phase rate coding in the basal forebrain

David Tingley, Andrew S. Alexander, Laleh K. Quinn, Andrea A. Chiba, Douglas Nitz*

*Corresponding author. Email: dnitz@ucsd.edu

Published 1 August 2018, *Sci. Adv.* **4**, eaar3230 (2018)
DOI: 10.1126/sciadv.aar3230

This PDF file includes:

Supplementary Figure 1

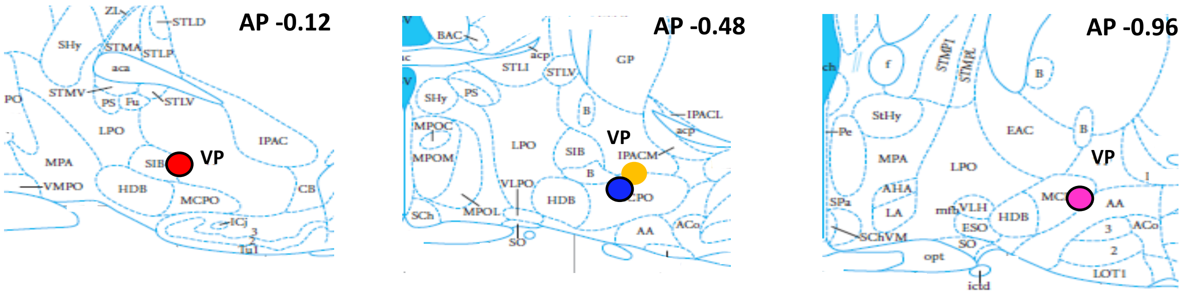

Fig. S1. Summary of LFP and multiple single-neuron recording sites in BF. Colored circles depict different animals. Black rings depict recordings made in left hemisphere.

Supplementary Figure 2

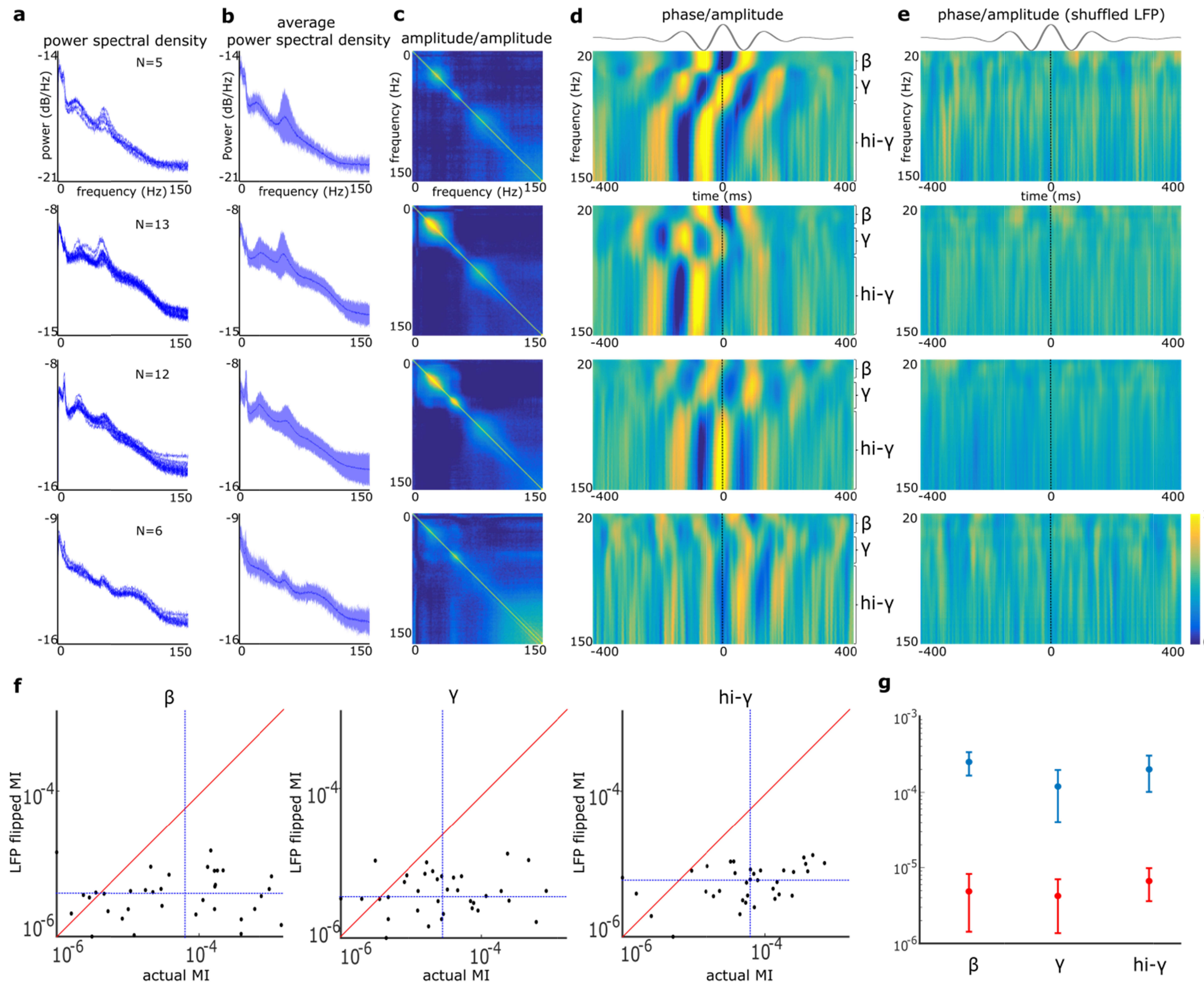

Fig. S2. Theta, beta, gamma, and hi-gamma frequencies are observed across multiple recording days and animals. (**A**) Power spectral density plots are shown for 5, 13, 12, and 6 recordings in individual animals. (**B**) The average power spectral density of all recording days, with the transparent shading representing two standard deviations. (**C**) Amplitude/amplitude correlations for each animal (color axis 0-1). (**D**) Theta frequency phase/amplitude coupling for each animal. For each frequency (y-axis) 800 millisecond windows of the wavelet transform, aligned relative to a peak in the theta phase, were averaged to get the mean fluctuation in power relative to the peak in theta. Each frequency was then z-scored to show average fluctuations at all frequencies (color axis -3 to 3) (**E**) Randomized phase/amplitude control. The same procedure as in fig. S2D was used, but after the theta-band-filtered signal used to define theta oscillation phases was reversed in time relative to wavelet transforms (color axis -3 to 3). (**F**) Tort's modulation index (MI) was used to quantify phase/amplitude coupling across recordings. For each frequency band, Tort's modulation index was calculated for the entire recording. As a control, the LFP phases were flipped in direction relative to the amplitudes, and Tort's modulation index was recalculated. Scatter plots are the MI scores for each recording and its flipped control. Dashed blue lines represent the median across recordings. (**G**) Summary data for mean MI scores and mean flipped direction MI scores (error bars are +/- 1 standard deviation).

Supplementary Figure 3

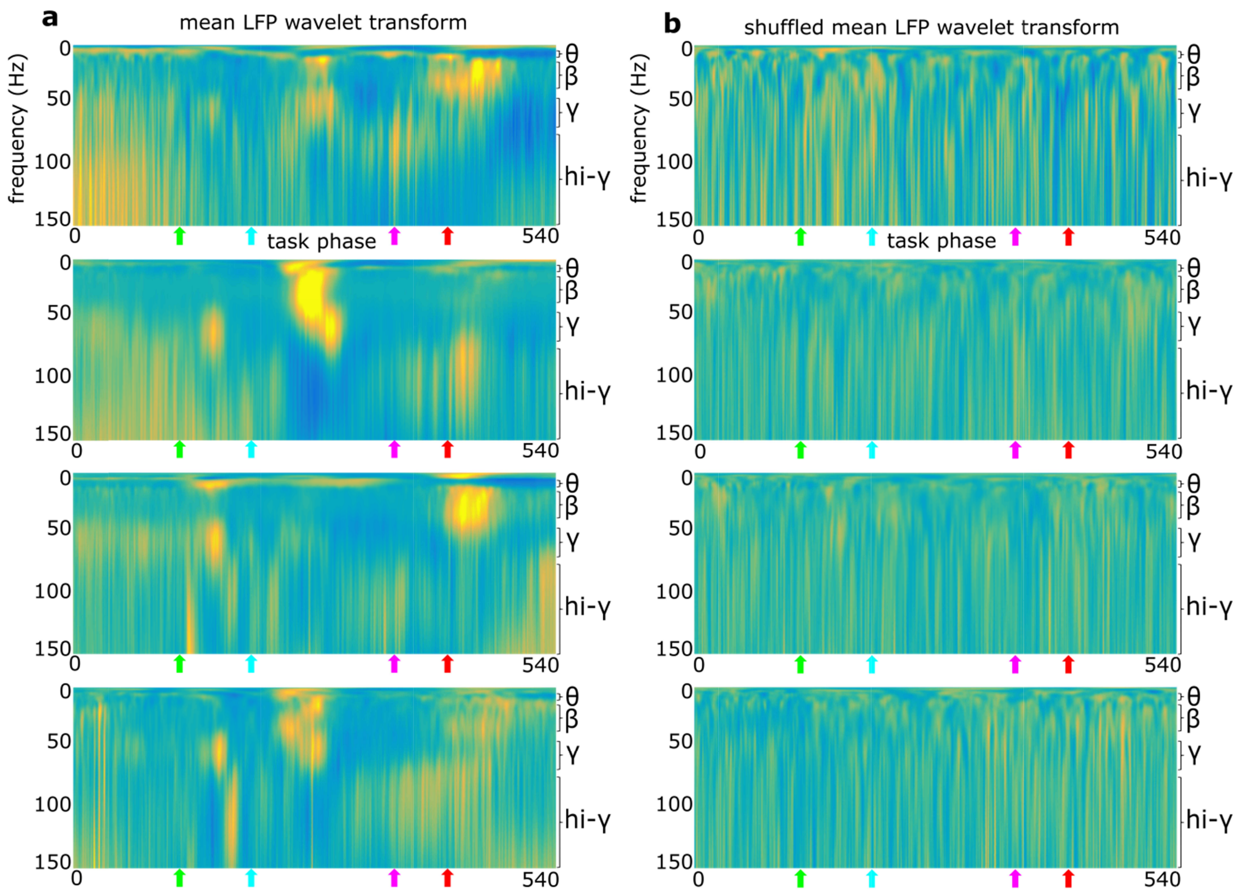

Fig. S3. Average wavelet transform of LFPs during selective attention task. (**A**) Average wavelet transform for all trials for each animal (5, 13, 12, and 6 recordings). Green, cyan, magenta, and red arrows demark, respectively, the light flash, nose-poke, plate-cross and stop/reward epochs of the task. All frequencies are z-scored, color axis is from -3 to 3(**B**) Randomized average wavelet transform for each animal. A number of randomly selected segments of LFP, matching the number and duration of the actual trials was used.

Supplementary Figure 4

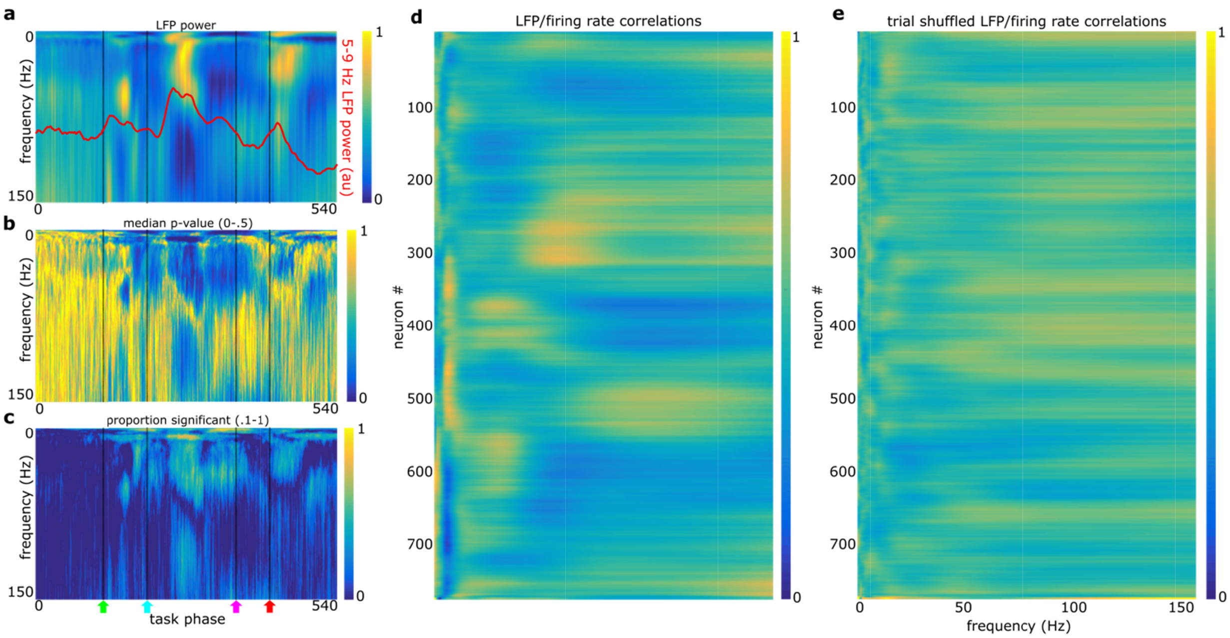

Fig. S4. Firing rate/LFP correlation control. (**A**) Average wavelet transform of local field potentials recorded during the selective attention task. Changes in local field potential power during the task can be observed across all four frequency ranges; theta (4-9 Hz; mean shown as red line), beta (20-35 Hz), gamma (45-60), and high gamma (80-150 Hz). All frequencies (rows) are individually maximum-normalized (color axis is 0-1) to visualize changes across the spectrum of frequencies present. (**B**) Median p-value across recordings (KS-test) for LFP power fluctuations compared with randomly selected equal length segments from the recording (**C**) Proportion (color axis 0-1) of recordings with LFP power fluctuations that were significantly different from equal length segments randomly selected from the recording for all frequencies (1-150 Hz) and task epochs (1-540). Note that both significant increases, and decreases (hi-gamma during return), in power are observed during specific task epochs. KS-test $p<0.05$ (**D**) Actual mean firing rate / LFP power correlations (color axis: 0-1) as seen in Fig. 2G**.** (**E**) Example firing rate / LFP power correlations when trial order was shuffled (color axis 0-1). 100 iterations of this were used for statistical comparison with the actual LFP power fluctuations (fig. S3D).

Supplementary Figure 5

a

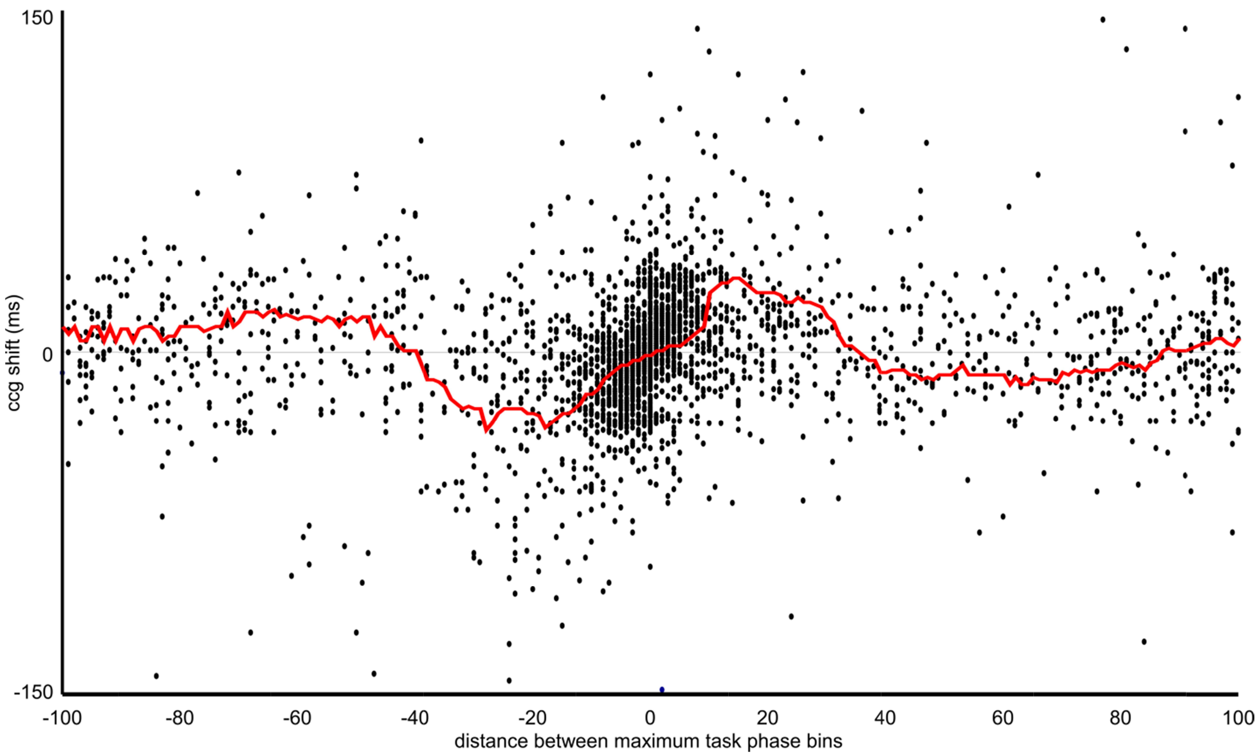

Fig. S5. Cross-correlogram offsets for simultaneously recorded neuron pairs correlate with distance between task epochs associated with maximal firing. Each dot shows the temporal shift to maximal cross correlation (y-axis) for spike times of a pair of simultaneously recorded neurons and the number of time normalized epochs (x-axis) between their peak firing rates relative to epochs of the selective attention task. Spike ordering persists despite overlap in the task epochs associated with peak task-related firing. The red line indicates the moving median of 20 consecutive task-epochs.

Supplementary Figure 6

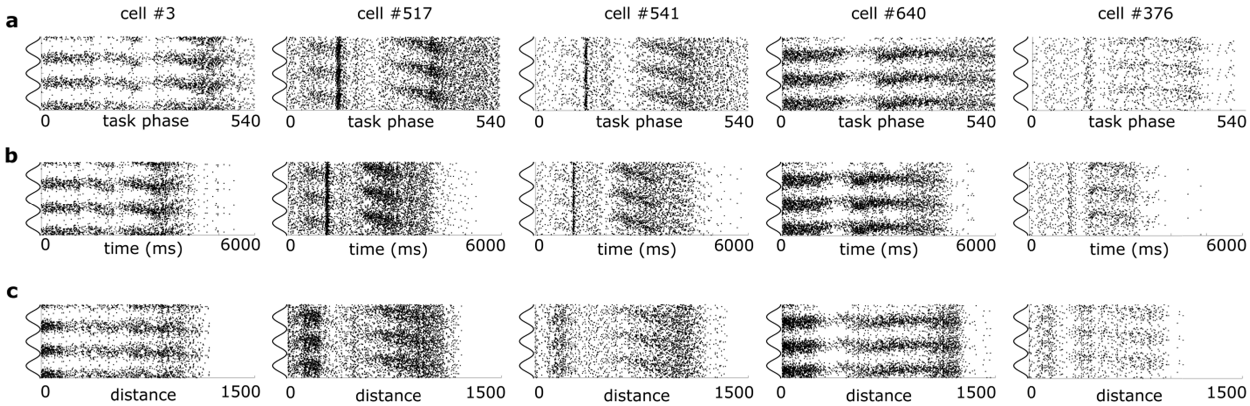

Fig. S6. BF neuron theta phase precession relative to task epoch, time, and space. (**A**) For each example neuron (columns), spike rasters were generated relative to theta phase and progression through task phases. (**B**) For each example neuron (columns), spike rasters were generated relative to theta phase and the amount of time passed within each trial. (**C**) For each example neuron (columns), spike rasters were generated relative to theta phase and the cumulative euclidean distance traveled within each trial.

Supplementary Table 1

Table S1. Phase-locking strengths do not correlate with burstiness or firing rate. For each frequency band, a correlation (Pearson's) is taken between the phase-locking resultant vectors and burstiness (top row) or firing rates (bottom row) for all neurons (N=780). R and P values are shown for each frequency band.

	Theta	Beta	Gamma	Hi-gamma
Burstiness (ISI_{1-50}/ISI_{51-250})	**R=.04, p=.29**	**R=-.05, p =.18**	**R=-.06, p=.12**	**R=-.05, p=.16**
Mean Rate	**R=-.04, p=.23**	**R=-.01, p= .89**	*** R=-.08, p=.02**	**R=-.06, p=.08**

Supplementary Table 2

Table S2. Phase-locking resultants do not correlate with task phase–specific firing or power/rate correlations. (**A**) Three groups of neurons when clustering (K-means) was performed on power/rate correlations (Fig. 3F right column). No group of neurons had a distribution of phase-locking resultant vectors that was significantly different from a randomly selected equal number of neurons (**B**) Three groups of neurons when clustering (K-means) was performed on task-phase specific firing patterns (Fig. 3F left column). No group of neurons had a distribution of phase-locking resultant vectors that was significantly different from a randomly selected equal number of neurons.

A

Categorized by rate/power correlation

	Theta	Beta	Gamma	Hi-gamma
Cluster 1 (N=388)	P=.54	P=.84	P=.98	P=.72
Cluster 2 (N=138)	P=.12	P=.70	P=.28	P=.27
Cluster 3 (N=254)	P=.69	P=.56	P=.18	P=.80

B

Categorized by mean rate over task phases

	Theta	Beta	Gamma	Hi-gamma
Cluster 1 (N=263)	P=.80	P=.38	P=.80	P=.68
Cluster 2 (N=262)	P=.99	P=.98	P=.52	P=.92
Cluster 3 (N=255)	P=.73	P=.95	P=.12	P=.20